TCR-peptide contact profile determines immunogenicity in pathogen/tumor-derived MHC-I epitopes.

Authors: Masato Ogishi[1, 2*] and Hiroshi Yotsuyanagi[2]

Affiliations:

[1] National Center for Global Health and Medicine Hospital, Tokyo, 162-8655, Japan

[2] Department of Infectious Diseases and Applied Immunology, Research Hospital, The Institute of Medical Science, The University of Tokyo, Tokyo, 108-0071, Japan

* To whom correspondence should be addressed: Masato Ogishi (oogishi-tky@umin.ac.jp)

One Sentence Summary: Accurate epitope prediction was achieved via machine learning by incorporating TCR-peptide contact profiles.

Keywords: Epitope prediction, T cell receptor repertoire, amino acid contact potential, machine learning

Conflict of Interest (COI): The authors declare no conflicts of interest.

Abstract

Computational methodologies to predict epitopes for cytotoxic T lymphocytes (CTLs) will galvanize vaccine research and pave the way toward targeted immunotherapy of infections and cancer. However, the classification of immunogenic epitopes and non-immunogenic major histocompatibility complex (MHC) class I ligands *in silico* has yet to attain sufficient accuracy. Here, we demonstrated highly accurate epitope prediction by a machine learning-based classifier incorporating T cell receptor (TCR)-peptide contact profiles, with an accuracy of 0.77 and an area under the curve of 0.84 in hold-out validation. Predictive accuracy was retained for five major human leucocyte antigen supertypes. Successful prediction using independent datasets of viral epitopes and tumor neoepitopes was demonstrated. Collectively, this is the first study demonstrating accurate and generalizable CTL immunogenicity prediction from the TCR-peptide axis. The R package *Repitope* was implemented to maximize code reusability. Prospective validation in vaccination and/or cancer immunotherapy cohorts is warranted.

Introduction

The adaptive immune system is driven by antigen recognition. The capability of triggering immune responses is termed 'immunogenicity'. Antigens are processed into fragments of peptides by proteasomes, and coupled to major histocompatibility complex [MHC; also called the human leucocyte antigen (HLA) in humans] molecules on the surface of antigen-presenting cells (APCs). Antigenic peptides presented by MHC-bearing cells are called MHC ligands. Naïve T cells interact with the MHC ligands (MHCLs) via their receptor (T cell receptor, TCR), and successful recognition activates them to initiate subsequent immunological orchestration(*1*). Immunogenic MHCLs are termed 'epitopes'. Conversely, being MHCLs does not ensure immunogenicity(*2*).

Acquired immunity plays an indispensable role in rejecting both pathogens and tumors. Accumulating evidence is shedding light on mutation-derived epitopes, or neoepitopes, as the targets of anticancer T cell immunity. First, the efficacy of immune checkpoint inhibitors correlates with tumor mutational burden(*3–6*). Second, mismatch-repair deficiency, which increases the overall genomic instability and tumor mutational burden, has been shown to predict a better outcome in patients receiving checkpoint blockade therapy(*7*), which eventually led to the FDA approval of the first pan-cancer efficacy biomarker(*8*). Third, the presence of neoepitope-specific T cells in

52 patients has been established(*9–11*). Finally, even outside the context of immunotherapy,
53 a heavier mutational burden has been shown to predict a longer overall survival through
54 the meta-analysis of genomic sequencing datasets from studies of six tumor types(*12*).
55 Collectively, these observations led to the unprecedented progress of precision
56 immunotherapy initiatives in oncoimmunology. However, personalized anticancer
57 immunotherapy is still at a nascent stage, in important part owing to the lack of a fast and
58 scalable methodology to screen potent neoepitopes. The test-one-by-one strategy is not
59 feasible given the heavy mutational burden observed in most types of cancer, and, albeit
60 extensively studied, immunoinformatics has achieved only minimal success to date in
61 predicting potent neoepitopes from their genomic profiles(*13*).

62 Two types of computational tools have been explored for applications in epitope
63 prediction. The first type predicts properties in the processes involved in antigen
64 presentation, including antigen processing, peptide transport, and the affinity and stability
65 of the MHC-peptide complex (*14–17*). A limitation of this approach is the high false
66 discovery rate in terms of immunogenicity (i.e., only a small fraction of the peptides
67 predicted and subsequently shown to bind to MHC are actually recognized by T cells and
68 elicit effective responses). The second category of tool used for epitope discovery is
69 aimed at the direct prediction of immunogenicity. Several immunoinformatic tools have

70 been proposed for the prediction of MHC class I (MHC-I) epitopes, which activate
71 cytotoxic T lymphocytes (CTLs) (*18–23*). However, none of them has demonstrated
72 adequate predictive performance in validation datasets, or has been successfully applied
73 to real-world datasets such as tumor neoepitope sequences obtained from immune
74 checkpoint inhibitor clinical trials.

75 Epitopes, by definition, are recognized by T cells via TCRs. However, in contrast to
76 the MHC-peptide axis, the TCR-peptide axis has yet to be thoroughly examined in the
77 context of immunogenicity. Exceptional research led by Chowell et al. demonstrated that
78 immunogenicity prediction was improved by incorporating hydrophobicity at TCR
79 contact residues(*23*). However, their model focuses on the biochemical properties of
80 MHC-I-loaded peptides but does not specifically address TCR-peptide interactions
81 themselves. On the other hand, a groundbreaking study conducted by Strønen et al. shed
82 light on the TCR-dependent nature of peptide immunogenicity in the context of
83 oncoimmunology(*24*). They showed that naïve T cell repertoires of healthy blood donors
84 were able to trigger effective immune responses against a variety of neoepitopes isolated
85 from cancer patients treated with immune checkpoint inhibitors. Many of the targeted
86 neoepitopes were overlooked by autologous tumor-infiltrating lymphocytes *in vivo*.
87 Furthermore, patient-derived T cells transformed with the appropriate donor TCR

88 successfully invigorated anti-neoepitope immunity. Their results suggest that even
89 MHCLs non-immunogenic to autologous TCRs can serve as epitopes if recognized by
90 appropriate TCRs.

91 We started the whole project aiming at unveiling the enigma of the
92 immunogenicity on MHC-I-loaded peptides on the basis of the following hypothesis:
93 are peptides stably interacting with the host TCR repertoire more likely to be
94 immunogenic? If this is the case, prediction of peptide immunogenicity may be
95 significantly improved by incorporating the TCR-peptide axis. Given that human TCR
96 repertoires are evolutionarily optimized so as to effectively combat pathogens and
97 cancers, we utilized a pooled human TCR repertoire sequenced from the commercial
98 RNA of peripheral blood $CD8^+$ T cells for reference. We defined repertoire-wide
99 TCR-peptide contact profiles (rTPCP) using amino acid pairwise contact potential
100 (AACP) scales to quantitatively parametrize TCR-peptide interactions to classify
101 epitopes and MHCLs through a machine learning (ML) approach. Our initial model
102 achieved unprecedented accuracy in hold-out validation. When the rTPCP definition
103 was modified to incorporate position-specific effects (mrTPCP), comparable accuracy
104 was achieved with just one AACP scale. Prediction was not biased for at least five HLA
105 supertypes. Permutation of peptide sequences, but not TCR sequences, undermined

106 predictive accuracy. Successful prediction was demonstrated using independent
107 epitope/MHCL datasets of viral and tumor origin. Moreover, using a mutational
108 landscape dataset obtained from checkpoint inhibitor trials, a correlation between
109 predicted neoepitope burden and clinical outcome was shown. Overall, this is the first
110 study demonstrating a highly accurate and generalizable epitope prediction by
111 integrating the TCR-peptide axis. The codes for rTPCP and mrTPCP analysis were
112 compiled into the R package *Repitope* (https://github.com/masato-ogishi/Repitope/).
113 Prospective validation of this tool in independent cohorts of vaccination and cancer
114 immunotherapy is necessary to evaluate its possible clinical applicability.

115

116 # Results

117 **Preparation of pooled human TCR repertoire dataset**

118 First, we screened public databases such as Sequence Read Archive, but failed to
119 find a suitable human TCR sequence dataset. Therefore, we generated an in-house TCR
120 repertoire data by sequencing the variable regions of TCR β chains (TCR-Vβ) from
121 commercially available pooled human peripheral $CD8^+$ T cells. Among the three
122 complementarity-determining regions (CDRs), we focused on CDR3, because it has the
123 largest diversity among CDR regions, and CDR1 and CDR2 are primarily involved in the
124 recognition of MHC, not the ligand presented(*1*). Rarefaction analysis estimated the total
125 CDR3 clonotype diversity be approximately 1500, out of which 872 unique clonotypes
126 were identified (fig. S1). No apparent bias in CDR3 length or Variable (V) and Junction
127 (J) segment usage was observed (fig. S2).

128 **Immunogenicity prediction from repertoire-wide TCR-peptide contact profiles**
129 **parametrized using amino acid contact potentials**

130 Immunogenicity prediction model necessitates quantitative parametrization of the
131 likelihood that a given peptide stably interacts with a given set of TCRs. Although
132 molecular dynamics simulation would be the most accurate method, it is not appropriate

133 because of its high demand for computational power; our goal is to construct a "portable"
134 prediction framework that can be run on ordinary desktop computers. To simplify the
135 framework, we adopted a sequence-based prediction strategy using AACPs listed in the
136 AAIndex database(*25*) (http://www.genome.jp/aaindex/AAindex/list_of_potentials) as
137 the measurement of energetic stability, or the decrease in free energy, of TCR-peptide
138 interaction. We hereby propose the concept of rTPCP, where a given peptide contacts
139 with all TCRs in a given repertoire with varying contact potentials (Fig. 1; see
140 Supplementary Materials and Methods for details). Using the rTPCP variables, we
141 attempted ML-based classification of MHCL peptides into immunogenic (functional
142 epitope) and non-immunogenic subsets. We utilized the peptide dataset compiled by
143 Chowell et al., which contains 7582 distinct human peptides (*23*). Preliminary analyses
144 suggested support vector machine (SVM) as the most accurate and balanced algorithm.
145 As an initial attempt, we focused on 450 epitopes and 450 ligands restricted on human
146 leucocyte antigen A2 (HLA-A2). We retrieved 35 AAIndex AACP scales (table S1) to
147 calculate rTPCP variables. To our surprise, the resultant SVM-based immunogenicity
148 prediction model achieved an unprecedentedly high predictive performance in the
149 hold-out validation dataset [accuracy, 0.81; 95% confidence interval (CI), 0.76 to 0.86;
150 receiver operating characteristic (ROC) area under the curve (AUC), 0.87; 95% CI, 0.83

151 to 0.91] (Fig. 2A). Four additional iterations using different random seeds yielded
152 comparable results (table S2).

153 One caveat of ML-based prediction is over-parametrization, which may lead to
154 model instability and limited generalizability, as is the case for our model (2520 rTPCP
155 variables against 900 HLA-A2-restricted peptides). Variable importance analysis
156 revealed that the AAIndex AACP scale MIYS990106, which represents inter-residue
157 pairwise contact energies(*26*), yielded the most consistently important variables (fig.
158 S3). Therefore, we retrained the SVM-based classifier solely using the
159 MIYS990106-derived rTPCP variables. This time, we included a full set of
160 epitopes/MHCLs in the dataset to maximize overall data size, resulting in a matrix with
161 72 variables for 7575 distinct peptides. The model achieved considerably high
162 performance despite the relatively small number of variables (accuracy, 0.75; 95% CI,
163 0.73 to 0.76; AUC, 0.81; 95% CI, 0.80 to 0.83) (Fig. 2B). Four additional iterations with
164 different random seeds yielded comparable results (table S3).

165 **Improved immunogenicity prediction by incorporating position-specific contact**
166 **profiles**

167 MHC-loaded peptides interact with TCRs at specific positions(*1*). The effects of
168 position-specific interactions may counterbalance each other in TPCP. To test this

169 hypothesis, we modified the rTPCP definition to incorporate position-specific
170 interactions (mrTPCP; schematically depicted in Figure 3). In this iteration, every TCR
171 was fragmented and pooled to generate a TCR fragment repertoire, and representative
172 statistics were calculated on a set of AACPs (see Supplementary Materials and Methods
173 for details). Because of the position-specific nature of the analysis, we limited the
174 subsequent analysis to 4738 unique nonapeptides in the Chowell dataset. The
175 SVM-based classifier trained from 187 mrTPCP variables outperformed our previous
176 rTPCP-based classifier (accuracy, 0.77; 95% CI, 0.75 to 0.79; AUC, 0.84; 95% CI, 0.82
177 to 0.86), with statistical significance [$p = 0.048$, according to the *roc.test* function
178 implemented in the *pROC* package(*27*)] (Fig. 4A). For comparison, the same dataset
179 was used to test three previously published immunogenicity prediction tools with
180 publicly available source code or web implementation. However, none of the tested
181 tools achieved similarly meaningful prediction; the accuracies were 0.56, 0.59, and 0.57
182 for POPISK(*19*), PAAQD(*20*), and EpitopePrediction(*28*), respectively.

183 The amino acid compositions of MHCLs are restricted by the HLA to which they
184 are coupled. Since our mrTPCP framework is not dependent on HLA information, it
185 might be useful for pan-specific immunogenicity prediction. To test this hypothesis,
186 4738 unique nonapeptides in the Chowell dataset were stratified based on their

187 corresponding HLA supertypes, and ROC analysis was conducted (Fig. 4B). The trained
188 classifier worked with no significant decrease in accuracy for at least five major HLA
189 supertypes (HLA-A1, A2, B15, B44, and B57) for which a sufficient amount of peptide
190 data was available.

191 Previous studies suggest that position-specific amino acid usage biases in
192 MHC-coupled peptides affect their immunogenicity(*21*, *23*). In our model, windows 1
193 and 2 seemed to be of higher importance, but no exceptionally important window was
194 identified (fig. S4). To further evaluate these position-dependent characteristics, we next
195 conducted sequence manipulation analysis; mrTPCP variables were calculated for
196 manipulated peptide sequences or using manipulated reference TCR repertoire
197 sequences. The classifier trained from authentic TCRs and peptides was then applied to
198 perform ROC analysis. Manipulation of TCRs led to a minimal decrease in AUC,
199 whereas manipulation of peptides led to a significant decrease in AUC (Fig. 4C).
200 Difference in amino acid compositions between epitopes and MHCLs was only of
201 partial predictive significance, indicating that position-specific or sequence-specific
202 features are the major determinants of immunogenicity.

203 Collectively, these observations suggest that the mrTPCP framework effectively
204 mimics the biological mechanisms of CTL immunogenicity, thereby providing a

205 promising methodology for accurate epitope prediction.

206 **Immunogenicity prediction using independent datasets**

207 Any pattern learned from one dataset is not always extendable to other datasets
208 constructed in different contexts. Therefore, we tested the performance of our
209 immunogenicity prediction model by utilizing independent datasets adopted from
210 previous publications(*4*, *10*, *24*, *29–32*), after removing peptides overlapping with those
211 in the Chowell dataset. As expected, randomly selected 10,000 MHCLs retrieved from
212 the Immune Epitope Database (IEDB) were predicted as either immunogenic or
213 non-immunogenic in an approximately 1:1 ratio, with a uniform distribution of
214 predicted probabilities (Fig. 5A and Table 1). In contrast, epitope datasets of viral and
215 tumor origin were significantly enriched with peptides predicted as epitopes ($p < 0.01$ by
216 Wilcoxon's rank sum test in comparison with randomly selected MHCLs from IEDB). It
217 is notable that 16 out of 22 (73%) well-defined neoepitopes and 22 out of 35 (63%) best
218 neoepitopes reported by Stronen et al. had probabilities of > 0.80 (Fig. 5A). With the
219 probability threshold of 0.80, our model also effectively classified the epitope/MHCL
220 dataset from various pathogens originally reported by Calis et al.(*21*) (accuracy, 0.71;
221 95% CI, 0.67 to 0.75; AUC, 0.77; 95% CI, 0.71 to 0.82) (Fig. 5B).

222 Encouraged by these observations, we next explored the possibility that our

223 immunogenicity prediction model improves the correlation between neoepitope burden
224 and clinical outcomes in checkpoint inhibitor trials. First, we adopted clinical and
225 mutational data from non-small cell lung carcinoma (NSCLC) patients treated with
226 pembrolizumab (n = 23)(*3*). We observed a slightly improved correlation between
227 neoepitope burden and progression-free survival (PFS) ($R = 0.55$, $p = 0.007$), compared
228 with the correlation between originally reported mutated peptide burden and PFS ($R =$
229 0.61, $p = 0.002$), although the improvement is not statistically significant as determined
230 by the methods implemented in the *cocor* package(*33*) (Fig. 6A). The PFSs of three
231 patients, namely, CA9903, CU9061, and SA9755, were better predicted (Fig. 6A). Next,
232 we analyzed clinical and mutational data from melanoma patients treated with
233 ipilimumab (n = 110)(*5*). Clinical benefit (CB) was defined as originally reported(*5*).
234 There were significant differences in both mutational burden and predicted neoepitope
235 burden between patients with and without CB (Fig. 6B). Overall, our results showed
236 that neoepitope burden predicted through the mrTPCP framework retains at least
237 comparable usefulness as a biomarker as compared with conventional mutational
238 burden, with greatly reduced number of neoepitope candidates, enabling more focused
239 approach in view of precision immunotherapy.

240 Finally, we compared estimated neoepitope burden across 21 tumor types in The

241 Cancer Genome Atlas (TCGA)(*34*). HLA-A-02:01 was chosen for subsequent analysis
242 as an example. Using the *EpitopePrediction* package(*28*), a total of 108,730 9-mer
243 MHCLs, of which 105,959 were unique, were identified. Immunogenicity prediction
244 was performed as described, with the probability threshold of 0.80. A total of 69,587
245 (64%) mutated peptides were predicted as neoepitopes. Skin cutaneous melanoma
246 (SKCM), lung squamous cell carcinoma (LUSC), and lung adenocarcinoma (LUAD)
247 were the three most MHCL-enriched, and neoepitope-enriched types of cancer (Fig. 7A).
248 There was a significant gene-by-gene variation of the ratio of neoepitope burden to the
249 MHCL burden (Fig. 7B). Mitochondrial enzymes (MT-CO1 and MT-ND4) and
250 olfactory receptors (OR2T2, OR4A5, OR4C16, OR4K2, OR5J2, and OR7D4) were the
251 genes that were particularly high-yield in terms of neoepitopes.

252 **R package implementation of immunogenicity prediction framework**

253 We implemented the R package *Repitope* to maximize code reusability. *Repitope*
254 contains datasets used in this study, functions to calculate rTPCP and mrTPCP variables
255 for user-provided peptide datasets and reference TCR repertoire data, and the mrTPCP
256 SVM classifier developed in this study. Source codes are deposited for public use at
257 GitHub (https://github.com/masato-ogishi/Repitope/).

258

Discussion

In this work, the accurate classification of epitopes and non-immunogenic MHC-I ligands was achieved by introducing the concept of repertoire-wide TCR-peptide contact profiles. Considering that current concepts of CTL epitope prediction are mostly focused on the peptide-MHC axis, it is of interest that our immunogenicity prediction model incorporating the TCR-peptide axis showed improved predictive capability over previous models.

We decided to use the dataset previously compiled by Chowell et al. for the following reasons. First, we eschewed compiling peptide datasets from scrach to avoid potential selection bias. Second, the dataset contains a sufficiently large number of human peptide data from IEDB, the largest and least biased data source available. Finally, the mutual exclusiveness of epitopes and MHCLs included in the dataset is ideal for model training and evaluation; the immunogenic CTL epitopes included were defined by T cell assays, and non-immunogenic MHCLs included were proven by MHC ligand elution assays, with any potentially immunogenic eluted ligand associated with autoimmunity or cancer being excluded. Consequently, the SVM classifier developed in this work successfully classified epitopes and MHCLs with unprecedented accuracy (Figs. 2 and 4). Moreover, our model also improved upon previous ones in that it employs smaller

277 number of variables(*19*, *22*) (fig. S3). Generally, ML classifiers using smaller numbers of
278 variables are preferable, since over-parametrization frequently causes ML algorithms to
279 "cheat", or to find variables distributed unevenly between the two classes in question just
280 because of stochastic fluctuation (with no generalizability for external data). Our
281 mrTPCP model employs only one AACP scale for parametrization, which resulted in 187
282 mrTPCP variables. This is a fairly small size when considering the number of input
283 peptides.

284 Our mrTPCP framework has two notable features: independence from HLA
285 specificity, and dependence on a reference TCR repertoire. First, pan-specific
286 immunogenicity prediction may be feasible, as it does not depend on HLA information.
287 We showed that our model worked with minimal performance reduction for at least five
288 major HLA supertypes (HLA-A1, A2, B15, B44, and B57), for which sufficient amount
289 of peptide data was available (Fig. 4B). This point could further be explored with more
290 immunogenicity data for various HLA alleles in the future. Second, the framework
291 requires reference TCR repertoire. The model discussed in this study relies on the pooled
292 TCR repertoire of German origin, which could be a source of bias. However,
293 immunogenicity could still be predicted with a minimal decrease in AUC, even when
294 using completely random sequences instead of TCR repertoire (Fig. 4C). Conversely,

295 manipulation of input peptide sequences resulted in a significant decrease in predictive
296 accuracy (Fig. 4C). These observations suggested that the mrTPCP framework is
297 primarily dependent on the inherent features of epitope sequence but not the reference
298 repertoire. Interestingly, peptide sequence permutation and randomization with relative
299 amino acid compositions retained led to moderately decreased AUC (0.68 and 0.64,
300 respectively), whereas completely random peptide sequences could not be classified
301 (AUC = 0.50). This is consistent with the previous research of Calis et al., in which an
302 AUC of 0.65 was obtained when residue-specific properties but not sequence-specific
303 properties were taken into consideration(*21*). Collectively, both amino acid composition
304 and sequence-specific features recapitulated by the mrTPCP framework are important in
305 determining peptide immunogenicity.

306 The regulatory mechanisms of CTL activation are asymmetric, and it is this
307 asymmetry that makes the construction of immunogenicity prediction models
308 complicated. The activation part is relatively simple; stable and strong interactions in the
309 TCR-peptide-MHC complex are the main driving force of T cell activation(*1*). In contrast,
310 there are several immunomodulatory systems outside the TCR-peptide-MHC axis
311 affecting the T cell activation process *in vivo*, including regulatory T cells (Tregs)(*35*),
312 CTL exhaustion mediated by chronic immune checkpoint signals, and the

313 immunosuppressive microenvironment engendered by solid tumors(*36*, *37*). Considering
314 this asymmetry, immunogenicity prediction models based solely on peptide sequence
315 may in principle yield some false positives. Therefore, our results should be recognized as
316 preliminary, warranting prospective validation to evaluate their clinical applicability.
317 That being said, however, eliminating candidates least likely to be immunogenic *in silico*
318 should greatly expedite research in targeted immunotherapy, and the findings in our
319 present study are indeed encouraging; epitopes of viral and tumor origin not included in
320 the training/testing dataset were successfully predicted with high sensitivity, whereas
321 predicted probabilities of MHCLs randomly retrieved from IEDB distributed almost
322 uniformly from 0 to 1 (Fig. 5 and Table 1). It is reasonable to assume a distribution of
323 levels of immunogenicity in the dataset of randomly selected MHCLs without T cell
324 assay-based annotation. Furthermore, we showed that the usefulness of neoepitope
325 burden as a biomarker for clinical outcome was not affected, or even slightly improved,
326 when candidate mutations were filtered using our prediction model (Fig. 6). One caveat to
327 be mentioned is its relatively low sensitivity in predicting HIV epitopes. In addition to the
328 "general" rules learned from the Chowell dataset which contains epitopes from various
329 sources, some additional rules may be critical for HIV-specific CTL immunity and could
330 be machine-learned with more data obtained specifically in the context of chronic HIV

331 infection.

332 Immune checkpoint inhibitors achieved revolutionary success in some types of
333 tumor including melanoma and non-small cell lung carcinoma (NSCLC)(*38–40*).
334 However, relatively few explanations have been proposed about the reason why these two
335 types of tumor are the most sensitive to checkpoint blockade. To address this, we
336 explored the entire TCGA cancer genome dataset(*34*). As anticipated, skin cutaneous
337 melanoma and NSCLC were most enriched with predicted MHCLs or neoepitopes (Fig.
338 7A). The ratio of predicted neoepitope to predicted MHCL significantly varied by
339 respective gene analyzed (Fig. 7B). Focusing on the high-yield genes such as
340 mitochondrial enzymes and olfactory receptors may expedite the development of
341 pan-cancer targeted immunotherapy.

342 Similarly to previous studies on immunogenicity prediction, this study has several
343 limitations. First, this is a retrospective observational study; no prospective identification
344 of novel epitopes is demonstrated. Thus, prospective validation is indispensable before
345 this model can be clinically applied. Second, the process of quantitative parametrization
346 of TCR-peptide interactions could further be optimized, as our window-based pairwise
347 interaction model might oversimplify the biophysicochemical nature of the
348 TCR-peptide-MHC interactions. In particular, the hypothesis that either a 4-mer or

349 5-mer window size is sufficient for recapitulating TCR-peptide interactions is not
350 experimentally verified, necessitating further exploration. Moreover, we limited our
351 modeling to TCR-Vβ, omitting TCR-Vα; this point could further be explored. Despite
352 these caveats, however, both the proposed framework of mrTPCP recapitulating the
353 biology of TCR-peptide interactions and the demonstrated robustness of
354 immunogenicity prediction represent noticeable progress toward fully unveiling the
355 mechanisms underlying CTL immunity, paving the way toward precision
356 immunotherapy against pathogens and cancer.

357 In conclusion, accurate epitope prediction was achieved through a machine
358 learning approach by incorporating TCR-peptide interactions parametrized using an
359 optimal amino acid pairwise contact potential scale. Unbiased prediction was
360 demonstrated for peptides coupled to multiple major HLA supertypes. The framework
361 was primarily reliant on the sequence-dependent features of the peptides, and only
362 minimally affected by the perturbation of the reference TCR repertoire. The resultant
363 classifier worked well for independent viral epitopes and tumor neoepitopes. These
364 findings not only provide valuable insights into the mechanisms underlying CTL
365 immunity, but could also bolster the ongoing precision immunotherapy initiatives. Code
366 reusability was maximized by publicly distributing the R package *Repitope*, in which

datasets and key scripts are bundled. Disease-specific, prospective cohort studies could be conducted to evaluate clinical usefulness in the future.

Materials and Methods

Study design

Research objectives. The purpose of this study was to construct a sequence-based epitope prediction model by incorporating TCR-peptide contact profiles.

Design. This is a retrospective, observational study. The entire analysis is exploratory; no predetermined experimental protocol was applied *a priori*.

Data collection. Peptide sequences accompanied by annotations on immunogenicity and other clinical profiles (if applicable) were manually retrieved from public database and previously published articles by the authors.

Data size. The optimal sizes of the epitope and MHCL datasets are unknown, since we hereby proposed a novel framework. Therefore, no statistical estimation was performed to predetermine sample size.

Computational analysis

All in-house computational analyses were conducted using R ver. 3.4.0 (https://www.r-project.org/) (*42*). The latest versions of R packages were consistently used. Key datasets and scripts were bundled as the R package *Repitope*, and publicly distributed in GitHub (https://github.com/masato-ogishi/Repitope/). Other scripts are available upon request.

388 **Preparation of pooled human TCR repertoire dataset**

389 TCR repertoire sequencing was carried out as previously described(*43*), except the
390 primers being used. Briefly, total RNA from $CD8^+$ T cells collected from donated
391 peripheral blood of German origin was purchased (Miltenyi Biotec) and used as the
392 source of a pooled TCR repertoire. Primers for human TCR-Vβ were adopted from
393 previously published work(*44*). All primers were synthesized by Life Technologies, and
394 a template-switching oligo (TSO) containing 5′ terminal unique molecular identifier
395 (UMI) and 3′ terminal guanidine locked nucleic acid (LNA) was synthesized by
396 Exiqon(*45*). The sequences of the oligonucleotides utilized in this study are summarized
397 in table S4. Reverse transcription with template-switching and semi-nested step-out PCR
398 were performed using SMARTScribe (Clontech) and KAPA2G Fast Multiplex PCR
399 master mix (Kapa Biosystems)(*46*). Amplified PCR products were gel-excised, repaired,
400 and re-purified. Paired-end libraries were prepared, and paired-end sequencing of 2 x 300
401 bp was performed using MiSeq (Illumina). UMI-guided de-multiplexing was performed
402 using MiGEC software in order to reduce the effect of PCR amplification bias(*47*). CDR3
403 regions were identified using IMGT/HighV-QUEST(*48*)
404 (https://www.imgt.org/HighV-QUEST/).

405 **Epitope/ligand dataset for training/testing immunogenicity prediction model**

406 The dataset primarily utilized in this study is originated from the research led by
407 Chowell et al(*23*). Any peptide derived from a mouse experiment was removed to create
408 a human-specific immunogenicity dataset. No additional data filtering was performed to
409 avoid deliberate peptide selection.

410 **Machine learning for immunogenicity prediction**

411 Machine learning (ML) procedures were streamlined using the *caret* package in
412 R(*49*). The hold-out validation strategy was adopted; the input dataset was randomly split
413 into training and testing subdatasets in a ratio of 2:1. The training subdataset was
414 preprocessed (i.e., centered and scaled) using the *preProcess* function in *caret*. Ten-fold
415 cross-validations (CVs) were repeated ten times to train classifiers. Testing subdataset
416 was preprocessed using the preprocessing model generated from the training subdataset,
417 and immunogenicity was predicted. Unless otherwise noted, the performance metric in
418 each testing subdataset was reported. As any ML algorithm is designed to self-optimize
419 through CVs, the performance metric obtained in the process of CVs is an optimized
420 value for the input dataset. Our true interest is the performance of the trained classifier
421 when applied to an external dataset not involved in either model training or optimization.
422 Preliminary assessment suggested that the support vector machine (SVM) was the best
423 algorithm. SVM has a long history of providing state-of-the-art, well-generalizable

424 predictions in various biological contexts(*50*). Four SVM methods, namely, *svmLinear*,
425 *svmPoly*, *svmRadial*, and *svmRadialSigma*, were tested. We chose *svmPoly* as the best
426 algorithm on the basis of various factors including accuracy, AUC, balance between
427 sensitivity and specificity, and the smoothness of the calibration curve. Accuracy was
428 calculated using the *confusionMatrix* function implemented in *caret*, and AUC was
429 calculated using either the *classifierplots* function in the *classifierplots* package, or the
430 *roc* and *auc* functions implemented in the *pROC* package(*27*).

431 **Epitope/ligand datasets for external validation**

432 The hold-out validation strategy is by itself not sufficient for evaluating the
433 generalizability of the ML classifier for external datasets. The ML algorithm, after all,
434 mines hidden patterns applicable across the training dataset. When the hold-out
435 validation strategy is adopted, training and testing subdatasets derived from a single
436 data source lie in a single context, and consequently, patterns learned from the training
437 subdataset is highly likely applicable to the testing subdataset. Therefore, the trained
438 classifier should be tested and validated with other external datasets constructed in
439 different contexts. In this study, the trained classifier may be biased, since
440 autoimmunity- and cancer-associated immunogenic peptides were excluded from the
441 epitope data, and pathogen-derived MHCLs were excluded from the MHCL data in the

442 Chowell dataset.

443 To independently assess the generalizability of the trained immunogenicity
444 prediction model, epitope datasets were collected from the following sources: (i)
445 hepatitis C virus (HCV) CTL epitopes
446 (https://hcv.lanl.gov/content/immuno/tables/ctl_summary.html), (ii) human
447 immunodeficiency virus type-I (HIV) CTL epitopes
448 (https://www.hiv.lanl.gov/content/immunology/tables/ctl_summary.html), (iii)
449 well-established tumor neoepitopes from multiple publications(*4*, *10*, *29–32*), (iv)
450 neoepitopes predicted to be the most stable MHC binders identified in the study by
451 Stronen et al.(*24*), and (v) all neoepitopes identified in the study by Stronen et al. For
452 comparison, we also obtained a human MHCL dataset from IEDB (http://www.iedb.org/).
453 Note that the MHCL data lacks T cell assay annotation, and thus the true ratio of 'epitopes'
454 to 'MHCLs' in the definitions discussed in this study is unknown. Moreover, we retrieved
455 the epitope/MHCL dataset originally reported by Calis et al(*21*). This dataset is suitable
456 for assessing the specificity of our immunogenicity prediction model, because it contains
457 experimentally validated non-immunogenic MHCLs, mostly originated from dengue
458 virus. Peptide sequences containing alphabetical characters other than those representing
459 20 authentic amino acid residues were removed. Any peptide contained in the Chowell

460 dataset was excluded. Datasets are available as supplementary data files (Data files
461 S1-S6).

462 **Correlation with clinical outcomes in checkpoint inhibitor trials**

463 Correlation between mutational landscapes and clinical outcome has been shown
464 in various tumor types in checkpoint inhibitor trials(*3–5*) To test the predictive
465 usefulness of neoepitope burden predicted through the proposed framework, we
466 re-analyzed mutational datasets from two studies(*3*, *5*). Datasets are available as
467 supplementary data files (Data files S7 and S8).

468 **Neoepitope burden across TCGA tumor types**

469 To assess the difference in neoepitope burden across tumor types, we analyzed
470 genomic datasets derived from The Cancer Genome Atlas project(*34*). For all advanced
471 stage (Stage III and Stage IV) tumors, mutation annotation format (MAF) files were
472 downloaded from the National Cancer Institute (NCI) Genomic Data Commons (GDC)
473 Data Portal (https://portal.gdc.cancer.gov/). Mutation data were parsed, and
474 nonapeptides harboring mutation were reconstructed by referencing the UniProt human
475 proteome (ID: UP000005640). HLA-A-02:01 is used as a representative allele, and the
476 binding stability of all nonapeptides were estimated using the *EpitopePrediction*

477 package(*28*). The dataset is available as a supplementary data file (Data file S9).

478 **Statistical analysis**

479 No variable distribution was assumed *a priori*, and data were presented as median
480 and interquartile range, unless otherwise stated. *P* values were reported unadjusted unless
481 otherwise stated. No accounting for missing data values is applicable. All statistical
482 analysis is exploratory; no predetermined experimental protocols were applied before
483 initiating the entire project. All statistical analyses were conducted in R.

484

Supplementary Materials

Supplementary Materials and Methods

Fig. S1. Clonotype rarefaction analysis in the reference TCR repertoire.

Fig. S2. Composition of the reference TCR repertoire..

Fig. S3. Exploration of AACP scales most important in the immunogenicity prediction models trained using rTPCP variables.

Fig. S4. Variable importance analysis of the immunogenicity prediction model trained using mrTPCP variables.

Table S1. AAIndex AACP scales used in this study.

Table S2. Performance evaluation of SVM classifiers with rTPCP variables from all AAIndex AACP scales.

Table S3. Performance evaluation of SVM classifiers with rTPCP variables from MIYS990106 AACP scale.

Table S4. Oligonucleotides used in this study.

Data file S1. HCV CTL epitopes.

Data file S2. HIV CTL epitopes.

Data file S3. Well-established tumor neoepitopes from multiple publications.

Data file S4. Best-predicted tumor neoepitopes reported by Stronen et al.

503 Data file S5. All neoepitopes reported by Stronen et al.

504 Data file S6. Pathogen-derived epitopes reported by Calis et al.

505 Data file S7. Tumor neoepitopes and clinical data reported by Rizvi et al.

506 Data file S8. Tumor neoepitopes and clinical data reported by van Allen et al.

507 Data file S9. Tumor neoepitope candidates identified from TCGA datasets.

508

509 # References

510 1. M. G. Rudolph, R. L. Stanfield, I. A. Wilson, How TCRs bind MHCs, peptides,
511 and coreceptors. *Annu. Rev. Immunol.* **24**, 419–66 (2006).

512 2. G. T. Gibney, L. M. Weiner, M. B. Atkins, Predictive biomarkers for checkpoint
513 inhibitor-based immunotherapy. *Lancet Oncol.* **17**, e542–e551 (2016).

514 3. N. A. Rizvi *et al.*, Mutational landscape determines sensitivity to PD-1 blockade
515 in non-small cell lung cancer. *Science (80-.).* **348**, 124–128 (2015).

516 4. A. Snyder *et al.*, Genetic Basis for Clinical Response to CTLA-4 Blockade in
517 Melanoma. *N. Engl. J. Med.*, 2189–2199 (2014).

518 5. E. M. Van Allen *et al.*, Genomic correlates of response to CTLA-4 blockade in
519 metastatic melanoma. *Science (80-.).* **350**, 207–211 (2015).

520 6. L. M. Colli *et al.*, Burden of nonsynonymous mutations among TCGA cancers
521 and candidate immune checkpoint inhibitor responses. *Cancer Res.* **76**, 3767–
522 3772 (2016).

523 7. A. D. Skora *et al.*, PD-1 Blockade in Tumors with Mismatch-Repair Deficiency.
524 *N. Engl. J. Med.*, 2509–2520 (2017).

525 8. K. Garber, Oncologists await historic first: a pan-tumor predictive marker, for
526 immunotherapy. *Nat. Biotechnol.* **35**, 297–298 (2017).

527 9. M. M. Gubin *et al.*, Checkpoint blockade cancer immunotherapy targets
528 tumour-specific mutant antigens. *Nature*. **515**, 577–581 (2014).
529 10. N. van Rooij *et al.*, Tumor Exome Analysis Reveals Neoantigen-Specific T-Cell
530 Reactivity in an Ipilimumab-Responsive Melanoma. *J. Clin. Oncol.* **31**, e439–
531 e442 (2013).
532 11. A. Gros *et al.*, Prospective identification of neoantigen-specific lymphocytes in
533 the peripheral blood of melanoma patients. *Nat. Med.* (2016),
534 doi:10.1038/nm.4051.
535 12. S. D. Brown *et al.*, Neo-antigens predicted by tumor genome meta-analysis
536 correlate with increased patient survival. *Genome Res.* **24**, 743–750 (2014).
537 13. Editorial, The problem with neoantigen prediction. *Nat. Biotechnol.* **35**, 97–97
538 (2017).
539 14. M. Nielsen, C. Lundegaard, O. Lund, C. Keşmir, The role of the proteasome in
540 generating cytotoxic T-cell epitopes: insights obtained from improved predictions
541 of proteasomal cleavage. *Immunogenetics*. **57**, 33–41 (2005).
542 15. T. Stranzl, M. V. Larsen, C. Lundegaard, M. Nielsen, NetCTLpan: pan-specific
543 MHC class I pathway epitope predictions. *Immunogenetics*. **62**, 357–368 (2010).
544 16. M. Nielsen, M. Andreatta, NetMHCpan-3.0; improved prediction of binding to

545 MHC class I molecules integrating information from multiple receptor and
546 peptide length datasets. *Genome Med.* **8**, 33 (2016).
547 17. M. Rasmussen *et al.*, Pan-Specific Prediction of Peptide–MHC Class I Complex
548 Stability, a Correlate of T Cell Immunogenicity. *J. Immunol.* **197**, 1517–1524
549 (2016).
550 18. C. W. Tung, S. Y. Ho, POPI: Predicting immunogenicity of MHC class I binding
551 peptides by mining informative physicochemical properties. *Bioinformatics*. **23**,
552 942–949 (2007).
553 19. C. W. Tung, M. Ziehm, A. Kamper, O. Kohlbacher, S. Y. Ho, POPISK: T-cell
554 reactivity prediction using support vector machines and string kernels. *BMC*
555 *Bioinformatics*. **12**, 446 (2011).
556 20. T. Saethang *et al.*, PAAQD: Predicting immunogenicity of MHC class I binding
557 peptides using amino acid pairwise contact potentials and quantum topological
558 molecular similarity descriptors. *J. Immunol. Methods*. **387**, 293–302 (2013).
559 21. J. J. A. Calis *et al.*, Properties of MHC Class I Presented Peptides That Enhance
560 Immunogenicity. *PLoS Comput. Biol.* **9** (2013),
561 doi:10.1371/journal.pcbi.1003266.
562 22. W. Zhang *et al.*, Accurate prediction of immunogenic T-cell epitopes from

563 epitope sequences using the genetic algorithm-based ensemble learning. *PLoS*
564 *One*. **10**, e0128194 (2015).
565 23. D. Chowell *et al.*, TCR contact residue hydrophobicity is a hallmark of
566 immunogenic CD8 + T cell epitopes. *Proc. Natl. Acad. Sci.* **112**, E1754–E1762
567 (2015).
568 24. E. Strønen *et al.*, Targeting of cancer neoantigens with donor-derived T cell
569 receptor repertoires. *Science (80-.).* **2288**, 1–11 (2016).
570 25. S. Kawashima *et al.*, AAindex: Amino acid index database, progress report 2008.
571 *Nucleic Acids Res.* **36**, 202–205 (2008).
572 26. S. Miyazawa, R. L. Jernigan, Self-consistent estimation of inter-residue protein
573 contact energies based on an equilibrium mixture approximation of residues.
574 *Proteins*. **34**, 49–68 (1999).
575 27. X. Robin *et al.*, pROC: an open-source package for R and S+ to analyze and
576 compare ROC curves. *BMC Bioinformatics*. **12**, 77 (2011).
577 28. Y. Kim, J. Sidney, C. Pinilla, A. Sette, B. Peters, Derivation of an amino acid
578 similarity matrix for peptide:MHC binding and its application as a Bayesian prior.
579 *BMC Bioinformatics*. **10**, 394 (2009).
580 29. B. M. Carreno *et al.*, A dendritic cell vaccine increases the breadth and diversity

581 of melanoma neoantigen-specific T cells. *Science (80-.).* **348**, 803–808 (2015).

582 30. E. Tran *et al.*, Immunogenicity of somatic mutations in human gastrointestinal

583 cancers. *Science (80-.).* **350**, 1387–1390 (2015).

584 31. L. Kong *et al.*, Structural basis of hepatitis C virus neutralization by broadly

585 neutralizing antibody HCV1. *Proc. Natl. Acad. Sci. U. S. A.* **109**, 9499–9504

586 (2012).

587 32. P. F. Robbins *et al.*, Mining exomic sequencing data to identify mutated antigens

588 recognized by adoptively transferred tumor-reactive T cells. *Nat. Med.* **19**, 747–

589 752 (2013).

590 33. B. Diedenhofen, J. Musch, Cocor: A comprehensive solution for the statistical

591 comparison of correlations. *PLoS One*. **10** (2015),

592 doi:10.1371/journal.pone.0121945.

593 34. K. Chang *et al.*, The Cancer Genome Atlas Pan-Cancer analysis project. *Nat.*

594 *Genet.* **45**, 1113–1120 (2013).

595 35. L. Wojciech *et al.*, The same self-peptide selects conventional and regulatory

596 CD4+ T cells with identical antigen receptors. *Nat. Commun.* **5**, 5061 (2014).

597 36. R. Eil *et al.*, Ionic immune suppression within the tumour microenvironment

598 limits T cell effector function. *Nature*. **537**, 539–543 (2016).

599 37. C. H. Chang *et al.*, Metabolic Competition in the Tumor Microenvironment Is a
600 Driver of Cancer Progression. *Cell*. **162**, 1229–1241 (2015).
601 38. J. D. Wolchok *et al.*, Nivolumab plus ipilimumab in advanced melanoma. *N.*
602 *Engl. J. Med.* **369**, 122–33 (2013).
603 39. M. A. Postow *et al.*, Nivolumab and Ipilimumab versus Ipilimumab in Untreated
604 Melanoma. *N. Engl. J. Med.* **372**, 2006–2017 (2015).
605 40. H. Borghaei *et al.*, Nivolumab versus Docetaxel in Advanced Nonsquamous
606 Non-Small-Cell Lung Cancer. *N. Engl. J. Med.* **373**, 1627–39 (2015).
607 41. M. Yadav *et al.*, Predicting immunogenic tumour mutations by combining mass
608 spectrometry and exome sequencing. *Nature*. **515**, 572–6 (2014).
609 42. R Core Team, R: A Language and Environment for Statistical Computing
610 (2016), , doi:ISBN 3-900051-07-0.
611 43. M. Ogishi, H. Yotsuyanagi, K. Moriya, K. Koike, Delineation of autoantibody
612 repertoire through differential proteogenomics in hepatitis C virus-induced
613 cryoglobulinemia. *Sci. Rep.* **6**, 29532 (2016).
614 44. J. D. Freeman, R. L. Warren, J. R. Webb, B. H. Nelson, R. A. Holt, Profiling the
615 T-cell receptor beta-chain repertoire by massively parallel sequencing. *Genome*
616 *Res.* **19**, 1817–24 (2009).

617 45. S. Picelli *et al.*, Smart-seq2 for sensitive full-length transcriptome profiling in
618 single cells. *Nat. Methods*. **10**, 1096–1098 (2013).
619 46. M. Matz *et al.*, Amplification of cDNA ends based on template-switching effect
620 and step-out PCR. *Nucleic Acids Res.* **27**, 1558–1560 (1999).
621 47. M. Shugay *et al.*, Towards error-free profiling of immune repertoires. *Nat.*
622 *Methods*. **11**, 653–655 (2014).
623 48. S. Li *et al.*, IMGT/HighV QUEST paradigm for T cell receptor IMGT clonotype
624 diversity and next generation repertoire immunoprofiling. *Nat. Commun.* **4**, 2333
625 (2013).
626 49. M. Kuhn, Building Predictive Models in *R* Using the caret Package. *J. Stat. Softw.*
627 **28**, 1–26 (2008).
628 50. W. S. Noble, Support vector machine applications in computational biology.
629 *Kernel Methods Comput. Biol.*, 71–92 (2004).
630 51. T. C. Hsieh, K. H. Ma, A. Chao, iNEXT: an R package for rarefaction and
631 extrapolation of species diversity (Hill numbers). *Methods Ecol. Evol.* **7**, 1451–
632 1456 (2016).
633 52. D. V. Bagaev *et al.*, VDJviz: a versatile browser for immunogenomics data. *BMC*
634 *Genomics*. **17**, 453 (2016).

Acknowledgments: We thank Dr. Takahashi of Leavanest, Inc. for technical assistance in MiSeq sequencing. We are also grateful to Dr. Couture-Cossette and Dr. Ueno for thoughtful advices. **Funding**: This work was supported by a Grant-in-Aid for Scientific Research (No. 30251234) from the Ministry of Education, Culture, Sports, Science and Technology, Japan, and by a Grant-in-Aid (No. HIV 28) from the Ministry of Health, Labor and Welfare, Japan. **Author contributions**: M.O. and H.Y. designed the study; M.O. performed computational analyses, prepared the figures and tables, and drafted the manuscript; M.O. and H.Y. wrote the manuscript. All authors critically discussed the results and their implications, and reviewed and approved the final version of the manuscript. **Competing interests**: The authors declare no competing financial interests. **Data and materials availability**: The TCR sequence dataset was deposited in the DDBJ Sequence Read Archive (DRA) under accession number DRA005827. The datasets used in this study, the trained immunogenicity prediction model, and key codes were bundled and publicly distributed as the R package *Repitope* on GitHub (https://github.com/masato-ogishi/Repitope/).

Figures

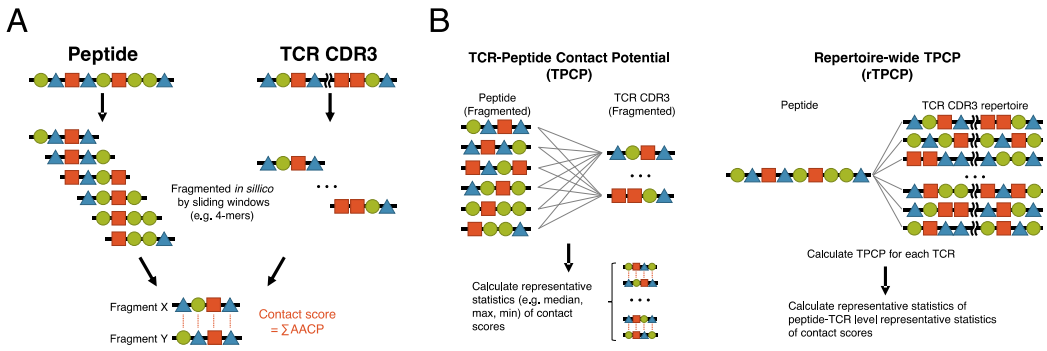

Figure 1. Schematic diagram of repertoire-wide TCR-peptide contact profile (rTPCP). Sequence-based modeling of TCR-peptide interactions is proposed. The interaction is restricted to a "window" of a fixed size, on the basis of the hypothesis that not all residues in the MHC-loaded peptide and TCR CDR3 are necessarily involved in the interactions. The energetic stability of the interactions is approximated as the summed amino acid pairwise contact potential (AACP). (A) TCR-peptide contact profile (TPCP) at a single TCR level. Both a peptide and a TCR CDR3 sequence are "windowed" in a sliding manner. Each fragment is paired, and the summed contact potential is calculated. TPCP is expressed as a set of representative statistics (e.g. median, maximum, minimum) of the set of inter-fragment contact potentials. (B) Repertoire-wide TPCP (rTPCP).

664 TPCPs were calculated against multiple TCR CDR3 sequences, and rTPCP is expressed

665 as a set of representative statistics of TPCPs.

666

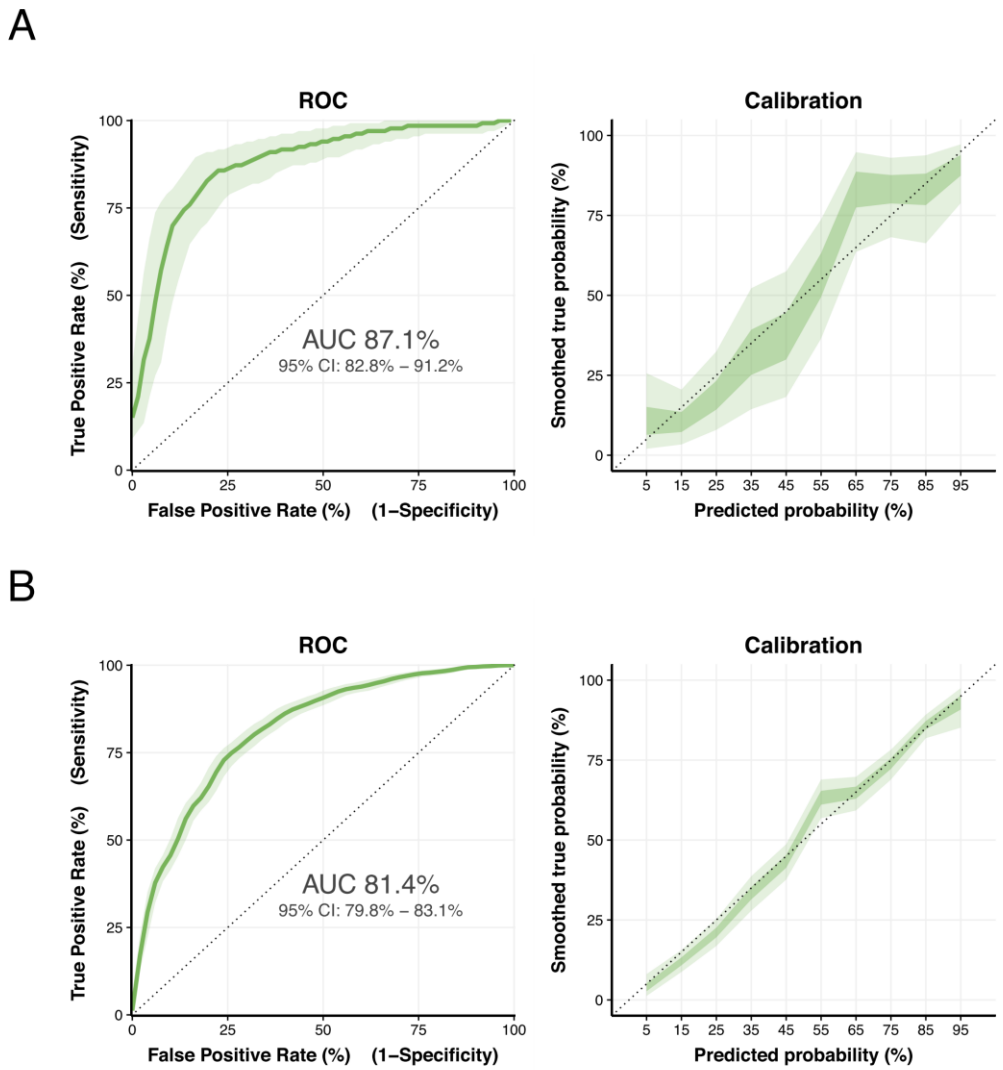

Figure 2. Immunogenicity prediction through rTPCP. (A) Representative ROC and calibration plots of the SVM classifier trained using rTPCP variables from all AACP scales. A total of 900 HLA-A2-restricted peptides (450 epitopes and 450 MHCLs) were randomly selected from the Chowell dataset, and split into training and testing subdatasets. The performance in the hold-out testing subdataset is shown. The AACP scales used are listed in table S1. (B) Representative ROC and calibration plots of the

SVM classifier trained using rTPCP variables from AAIndex MIYS990106. A full set of peptides in the Chowell dataset were used for model training and validation. Graphics were generated using the *classifierplots* package in R.

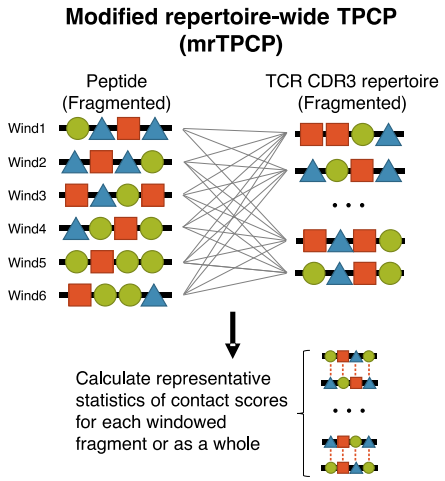

677 **Figure 3. Schematic diagram of modified rTPCP (mrTPCP).** All TCR sequences in

678 the reference repertoire are fragmented according to the fixed window size. A

679 position-specific peptide-derived fragment was matched against a set of TCR-derived

680 fragments. Representative statistics were calculated both in a position-specific and

681 position-blind (i.e., pooled) manner. Owing to the position-dependent nature of the

682 analysis, only nonapeptides (=9-mers) were considered in the subsequent analysis.

683

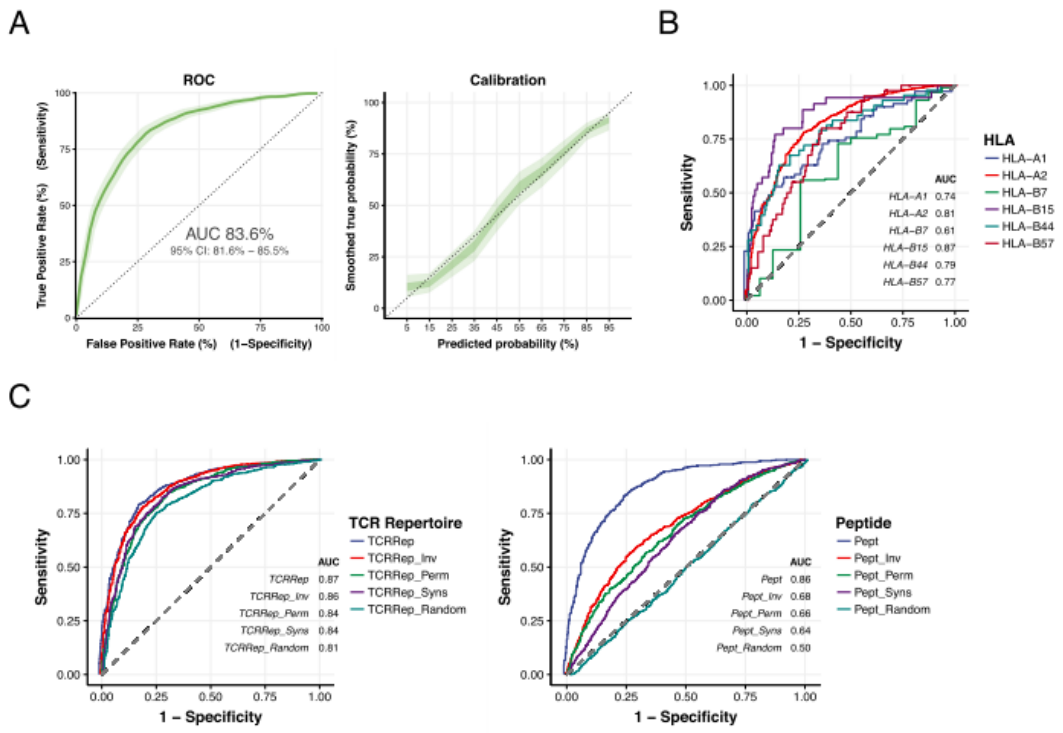

684 **Figure 4. Improved immunogenicity prediction using mrTPCP.** (A) ROC and

685 calibration plots of the SVM classifier trained using mrTPCP variables derived from

686 MIYS990106. See the legend of Fig. 2B and method sections for further details. (B)

687 HLA-stratified ROC analysis. The entire Chowell dataset was sorted according to their

688 HLA restriction, and six most data-rich HLA supertypes were selected for visualization.

689 (C) Sequence manipulation analysis. Either the input peptide sequences or the reference

690 TCR repertoire sequences were manipulated, and mrTPCP variables were calculated. The

691 authentically trained SVM classifier was applied. Inv, inversion of the sequence; Perm,

692 permutation of the sequence; Syns, randomly synthesized sequences with relative amino

693 acid frequencies retained. For peptides, amino acid frequencies of immunogenic and

694 non-immunogenic peptides were separately considered; Random, completely random

695 sequences. (B-C) AUC was calculated and graphics were generated using *pROC* and

696 *plotROC* packages in R, respectively.

697

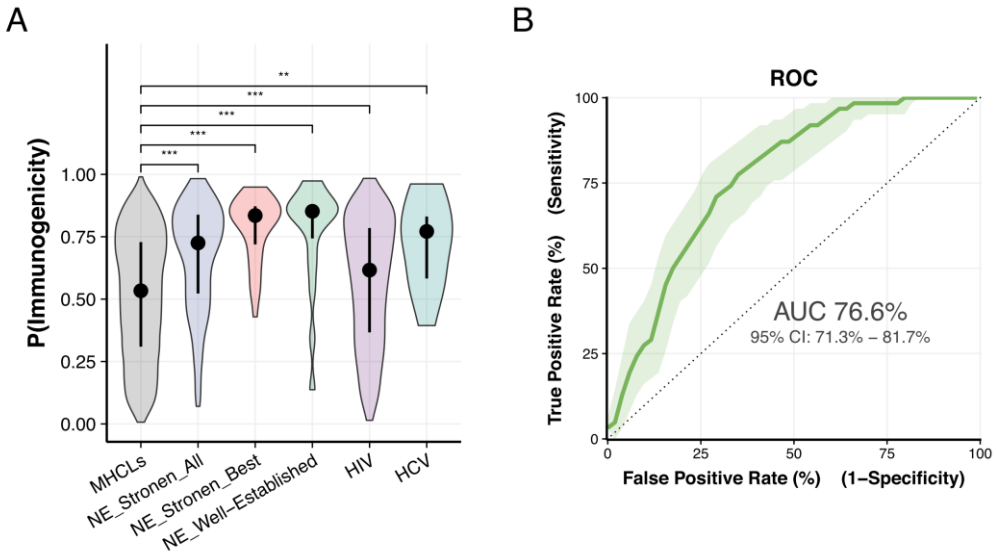

Figure 5. Immunogenicity prediction of independent datasets of viral epitopes and tumor neoepitopes. Peptide data were collected from various sources. Any peptide overlapping with those in the Chowell dataset was excluded. The probability of immunogenicity was estimated by applying the mrTPCP-based SVM classifier (Fig. 4A). (A) A metadataset of viral epitopes and tumor neoepitopes(*4*, *10*, *24*, *29–32*). Dots and bars represent the median and interquartile range, respectively. ***: $p < 0.001$, **: $p < 0.01$. *P* values were determined using Wilcoxon's rank sum test. NE, neoepitopes. (B) Epitope/ligand data originally reported by Calis et al.(*21*). The probability threshold was set to be 0.80.

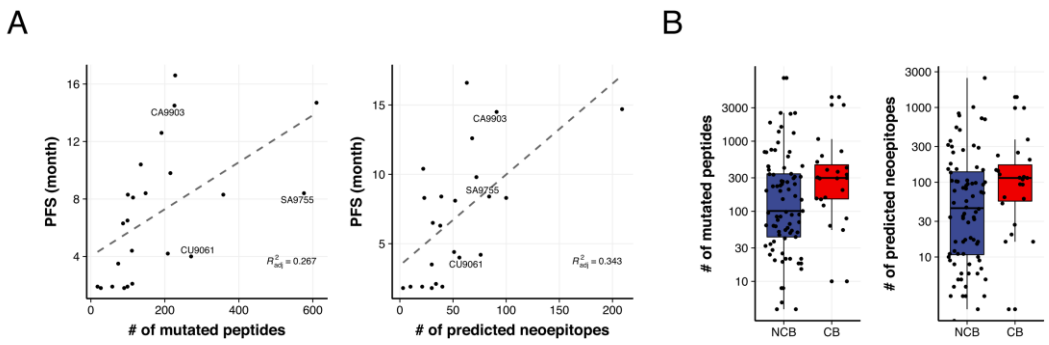

708 **Figure 6. Correlation between predicted neoepitope burden and clinical outcome in**

709 **checkpoint inhibitor trials.** The mrTPCP-based SVM classifier (Fig. 4A) was applied to

710 external datasets of tumor mutational landscapes obtained from checkpoint inhibitor

711 trials. We set the threshold of immunogenicity to be above 0.80, on the basis of the

712 observation that most of the well-established tumor neoepitopes exhibited probabilities of

713 higher than 0.80 (Fig. 5A) (A) Progression-free survival (PFS) correlated with mutational

714 burden/predicted neoepitope burden in non-small cell lung carcinoma (NSCLC) patients

715 treated with pembrolizumab(*3*). The three patients were labeled, for which scaled fitting

716 residuals decreased by more than 1 when the predicted neoepitope burden was used as a

717 correlate. Adjusted correlation coefficient ($R^2{}_{adj}$) was calculated using the *stat_poly_eq*

718 package.(B) Clinical benefit (CB) was associated with heavier mutational

719 burden/predicted neoepitope burden in melanoma patients treated with ipilimumab(*5*).

720 CB was defined as in the original paper(*5*). NCB, no clinical benefit.

721

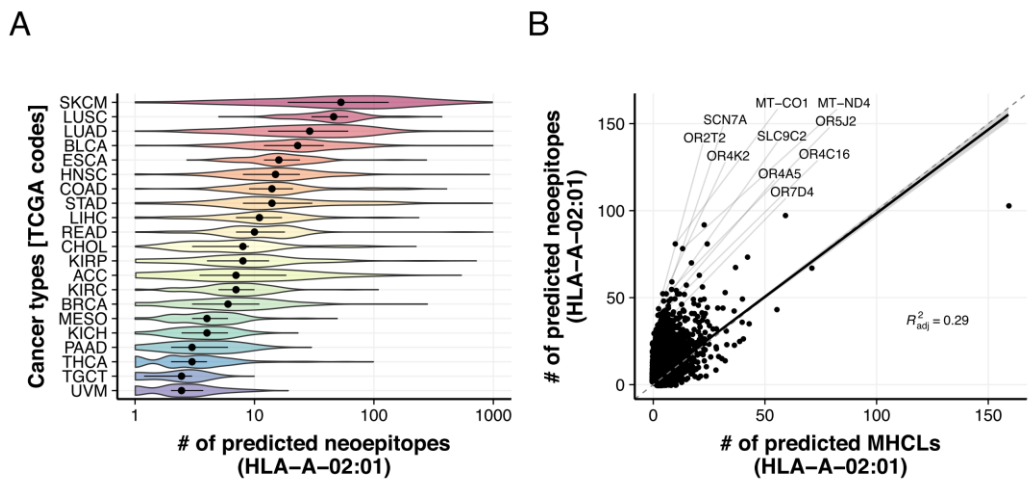

Figure 7. Neoepitope burdens in TCGA datasets. Mutation data were retrieved from all advanced stage tumors in The Cancer Genome Atlas (TCGA)(*34*). For the 105959 HLA-A-02:01-restricted nonapeptides predicted to be stable MHC binders, immunogenicity prediction was carried out. (A) Predicted neoepitope burden was visualized for the 21 tumor types registered in TCGA. SKCM, Skin Cutaneous Melanoma; LUAD, Lung adenocarcinoma; LUSC, Lung squamous cell carcinoma. For a complete set of abbreviation used in TCGA, visit the NCI Genomic Data Commons (https://gdc.cancer.gov/resources-tcga-users/tcga-code-tables/tcga-study-abbreviations). (B) The correlation between predicted MHCL burden and neoepitope burden per gene. HUGO symbols were depicted for genes enriched with neoepitopes. Enrichment was defined as fitting residuals being larger than 10 for the purpose of tidy visualization. Adjusted correlation coefficient was calculated using the *stat_poly_eq* package.

Tables

Table 1. Prediction results on datasets independent from training/validation data. Immunogenicity was predicted using the mrTPCP-based SVM classifier (Fig. 4A). Note that any peptide contained in the Chowell dataset was excluded. Unadjusted *p* values were calculated against the IEDB MHCL data as the negative control using the *prop.test* function implemented in R with continuity correction. N.A., not applicable.

Dataset	**Predicted Epitope**	***P* value**	**Data Source**
HCV CTL epitopes [n = 11]	10 (90.9%)	< 0.01	HCV immunology database (https://hcv.lanl.gov/content/immuno/tables/ctl_summary.html)
HIV CTL epitopes [n = 867]	545 (62.9%)	< 0.001	HIV molecular immunology database (https://www.hiv.lanl.gov/content/immunology/tables/ctl_summary.html)
Well-established tumor neoepitopes [n = 20]	18 (90.0%)	< 0.001	(*4*, *10*, *29–32*)
Tumor neoepitopes (Best) [n = 35]	34 (97.1%)	< 0.001	(*24*)
Tumor neoepitopes (All) [n = 492]	382 (77.6%)	< 0.001	(*24*)
IEDB MHC-I ligands [10,000 randomly selected]	5412 (54.1%)	N.A.	IEDB (http://www.iedb.org/)